

# Optical and Exciton Dynamical Properties of a Screw-Dislocation-Driven ZnO:Sn Microstructure

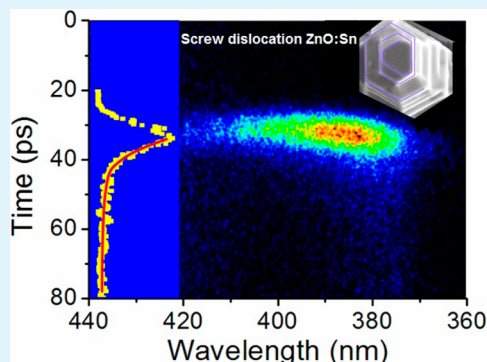
Jun Dai,\*<sup>†,‡</sup> Junfeng Lu,<sup>‡</sup> Fang Wang,<sup>†</sup> Jiyuan Guo,<sup>†</sup> Ning Gu,<sup>\*‡</sup> and Chunxiang Xu<sup>\*‡</sup>

<sup>†</sup>School of Mathematics and Physics, Jiangsu University of Science and Technology, Zhenjiang 212003, China

<sup>‡</sup>State Key Laboratory of Bioelectronics, School of Biology Science and Medical Engineering, Southeast University, Nanjing 210096, China

**ABSTRACT:** Screw dislocation plays a critical role in crystal growth and significantly affects the carrier dynamics process of luminescent semiconductor materials. In this paper, we report a novel screw-dislocation-induced ZnO:Sn hillock microstructure. The detailed growth process and possible formation mechanism of screw dislocation are demonstrated. The temperature-dependent photoluminescence reveals the free exciton recombination emission mechanism of the ZnO:Sn hillock microstructure. By comparing time-resolved photoluminescence spectra with those of two other samples without screw dislocations, it is found that the screw dislocation in the ZnO:Sn microstructures effectively decreases the carrier lifetime. In addition, UV Fabry–Perot lasing action is observed from the ZnO:Sn hillock microstructure, and the numerical simulation of the standing wave pattern and light intensity distribution further confirm the Fabry–Perot lasing mechanism. Therefore, ZnO:Sn can be utilized as a UV laser gain medium, and its optical properties can be modulated by screw dislocation.

**KEYWORDS:** screw dislocation, ZnO, carrier dynamics, photoluminescence, lasing



## 1. INTRODUCTION

Crystal growth is always a hot topic for many scientists in industry and academia. The growth mechanism and process for most of the functional materials have been revealed in the past several decades. It is well-known that dislocations and crystal defects can be formed intentionally or unintentionally in the crystal growth process. Early in the 1950s, Burton–Cabrera–Frank (BCF) theory concluded that screw dislocation plays a crucial role in crystal growth.<sup>1</sup> Usually perfect crystals only grow exceedingly slowly, and real crystals grow comparatively rapidly because they contain dislocations and other defects, which provide the necessary growth points and catalyst for structural transformation and long-range order formation. To date, screw dislocations in semiconductor crystalline media have attracted a growing interest from the application viewpoint for their profound influence on the optoelectronic properties of the host materials.

In the field of luminescent semiconductor materials, GaN has been widely investigated and successfully applied in the lighting industry. Researchers have found that screw dislocation can significantly shorten the carrier dynamic process, which is a critical property for a luminescent GaN device.<sup>2–7</sup> As another promising near-ultraviolet light-emitting and laser material, the cheap and easily grown group II–VI ZnO wide band gap semiconductor was regarded as the next-generation semiconductor material to substitute for GaN for its much larger exciton binding energy, which is helpful to present more stable ultraviolet light and lasing emission from the ZnO-based device.<sup>8,9</sup>

In the past decade, low-dimensional ZnO micro/nanostructures have attracted tremendous attention due to their unique physical properties and wide applications in functional micro/nanodevices. In addition, researchers have found that ZnO electronic properties can be effectively modulated by metal-doping, so AZO,<sup>10</sup> GZO,<sup>11</sup> IGZO,<sup>12,13</sup> and TZO<sup>14–19</sup> were widely investigated and applied in the electronic industry. Recently, the ZnO:Sn microstructure was fabricated by the vapor-phase transport method to change the optical and electrical properties.<sup>18,19</sup> Hitherto, a great number of novel ZnO-based micro/nanodevices, such as UV microlasers,<sup>8,9,20–22</sup> field effect transistors,<sup>23–25</sup> and photodetectors,<sup>26–28</sup> have been designed by using ZnO nanowires, nanotubes, nanotetrapods, nanoflowers, and nanodisks<sup>29</sup> as block units. However, the crystal growth mechanisms of those ZnO micro/nanostructures are still unclear, and few studies have investigated the role of defects and dislocations in the ZnO micro/nanostructures. Most importantly, it has not been studied how the screw dislocation in the ZnO microstructure affects the carrier dynamics process and nanodevices' performances. Recently, Prof. Jin's group found screw dislocation in the ZnO nanotube at low supersaturation conditions,<sup>30</sup> but the typical ZnO pyramid hillock structure induced by screw dislocation has not been reported. According to BCF theory, if the supersaturation is too low to form two-dimensional nuclei for layer by layer

Received: November 4, 2014

Accepted: May 26, 2015

Published: May 26, 2015

growth, the screw dislocation will be the dominant driving factor for crystal growth. As a result, it is desirable to realize screw-dislocation-driven ZnO growth if the supersaturation is controlled at an appropriately low condition, and reveal the screw-dislocation-related optical properties, which will shed light on how to modulate the ZnO devices' performances by crystal structure design.

In this work, we report a vapor-phase transport method to fabricate the screw-dislocation-induced ZnO:Sn microstructures at low supersaturation conditions, the temperature-dependent and time-resolved photoluminescence spectra of the ZnO:Sn microstructures are measured, and the exciton-related carrier dynamics process is discussed. In addition, the lasing action is observed from the ZnO:Sn hillock microstructure, and the lasing mode is further discussed on the basis of the numerical simulation. To explain the fast carrier dynamic process related to the screw dislocation and unintentional intrinsic oxygen vacancy defect, two undoped ZnO nanorod samples are fabricated to serve as reference samples. By comparison to the undoped ZnO nanorod array samples, the result indicates that the screw dislocation in the ZnO:Sn microstructure effectively accelerates the quenching of exciton emission and results in a very fast carrier decay process.

## 2. EXPERIMENTAL SECTION

ZnO:Sn microstructures were synthesized by a typical vapor-phase transport method. A mixture of ZnO powder (0.25 g), SnO<sub>2</sub> powder (0.023 g), and graphite (0.25 g) was ground and loaded in a ceramic boat to serve as the source material. The ceramic boat filled with the source material was placed in a quartz tube (length, 30 cm; diameter, 3 cm). A clean silicon substrate of 3 cm × 0.5 cm dimensions was placed 10 cm downstream from the ceramic boat. The tube loaded with the ceramic boat and the silicon substrate was pushed into a horizontal furnace. The temperature at the quartz boat was 1000 °C. In the reaction process, oxygen and argon gases were loaded into the horizontal furnace with flow rates of 10 and 150 sccm, respectively. To realize the low supersaturation condition for screw-dislocation-driven growth, the pressure in the tube was kept at 5 Torr by a mechanical pump. After 1 h of reaction, the product was deposited on the substrate.

Two reference samples (RS1, RS2) of the ZnO nanorod array without obvious screw dislocation were fabricated using the ZnO and graphite as source materials by the vapor transport method at different oxygen carrier gas flows (20 and 10 sccm). Other growth conditions (temperature, pressure, growth time) were the same as those for growing ZnO:Sn. RS1 has a low oxygen vacancy density, and RS2 has a high oxygen vacancy density.

The morphology of the as-grown sample was investigated by scanning electron microscopy (SEM), and the elemental distribution was measured by energy-dispersive spectrometry (EDS). The X-ray diffraction (XRD) pattern was obtained using Cu K $\alpha$  radiation ( $\lambda = 0.154$  nm).

To explicate the photoluminescence mechanism, the temperature-dependent photoluminescence of the ZnO:Sn microstructure was measured by a spectrometer using a 325 nm He–Cd continuous wave laser as the excitation source. To investigate the carrier dynamical process, time-resolved photoluminescence (TRPL) spectra of the ZnO:Sn microstructure were obtained at room temperature by an optically triggered streak camera system (CS410, Hamamatsu) at 295 nm from frequency doubling of the fundamental 120 fs pulses at 590 nm with a repetition rate of 76 MHz (Mira OPO, Coherent). To explicate the effect of screw dislocation and the oxygen vacancy defect on the carrier dynamics, the TRPL of RS1 and RS2 was measured for comparison with that of the ZnO:Sn hillock structure. Finally, Fabry–Perot lasing was observed from the hillock structure under the excitation of a 325 nm femtosecond laser. The standing wave pattern

and light field distribution in the Fabry–Perot cavity structure were simulated.

## 3. RESULTS AND DISCUSSION

SEM images of the ZnO:Sn microstructure with a Sn content of about 0.9% at different magnifications are shown in Figure 1.

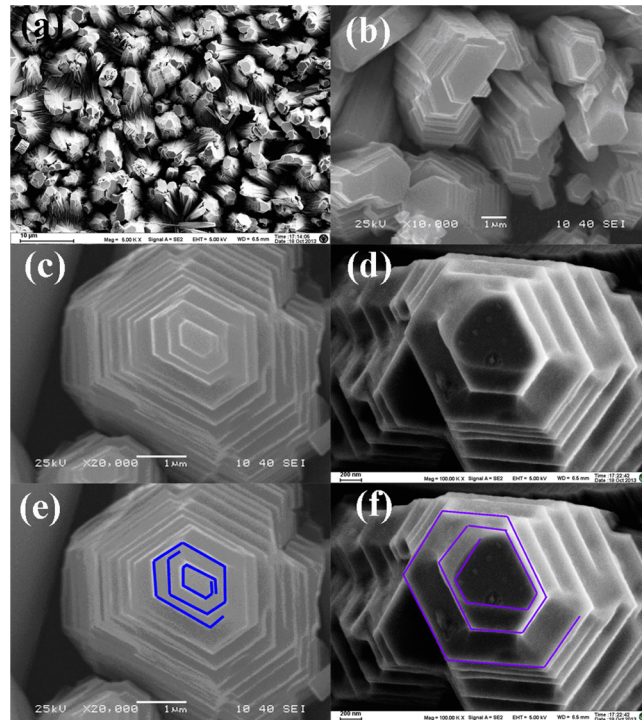


**Figure 1.** (a–d) SEM images of the ZnO:Sn microstructures at different magnifications. (e–f) Spiral screw dislocation edges (blue lines) of the ZnO:Sn microstructures shown in (c) and (d).

Different from the previously reported typical one-dimensional ZnO rod and wire structures with a symmetric hexagonal cross-section, the ZnO:Sn microstructure presents a hillock structure with a deformed hexagonal cross-section, which has an average height of 4  $\mu$ m. The average diameters of the base and the top surface of the hillock structure are about 5  $\mu$ m and 500 nm, respectively. A very interesting phenomenon is that the ZnO:Sn hillock seems to be composed by a multilayer structure with an average height of each layer step of about 20 nm, and more than 50% of the microhillocks present a spiral pattern on their top surface with their diameters decreasing continuously, as shown in the enlarged ZnO:Sn hillocks in Figure 1c,d. To clearly demonstrate the spiral step evolution path, the blue lines in Figure 1e,f denote the step structures of the two ZnO:Sn hillocks shown in Figure 1c,d. In the growth of semiconductor microstructures, thread dislocation, stacking faults, and other dislocations can coexist in the sample; however, a spiral step structure is usually regarded as a characteristic of screw-dislocation-driven growth. As for the formation mechanism of screw dislocation of the ZnO:Sn microstructure, Sn doping probably plays a critical role in forming the screw dislocation. Previous reports have revealed that metal doping can form the core of screw dislocations.<sup>6,31,32</sup> Similarly, we suggest that Sn atoms stack on the nanocrystal surface and substitute for the Zn atom in the growth process, but the Sn atom has a smaller radius than the Zn atom; maybe the doping of Sn forms an atom step which induces the initial screw dislocation. With

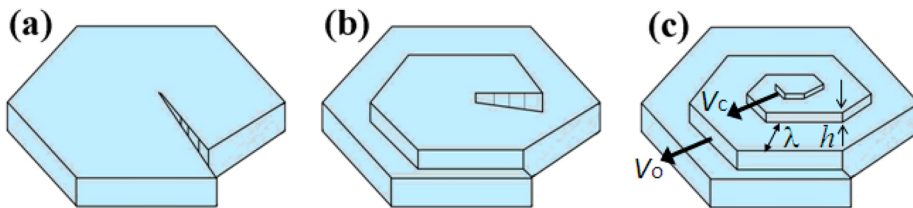


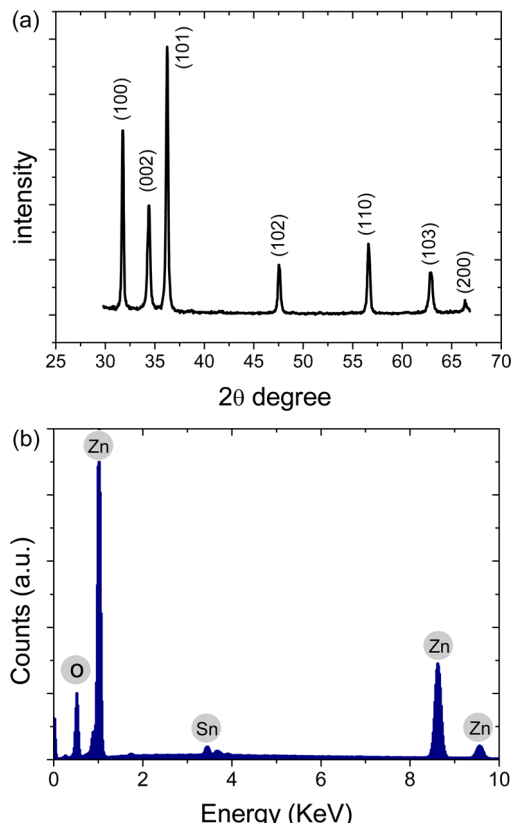
**Figure 2.** Schematic propagation of screw dislocation growth spirals.

growth continuing, the step spirals and presents the screw dislocation. Such a screw-dislocation-induced self-perpetuating growth spiral is schematically demonstrated in Figure 2. At the beginning of forming screw dislocation, a step was formed as shown in Figure 2a. With the growth continuing, the spiral step advances forward by the screw dislocation. Therefore, screw dislocation will result in the hillock structure as shown in Figure 2b. The hillock structure can be further understood from the step velocities at the core ( $v_c$ ) of the hexagon and at the outer edge ( $v_o$ ) as denoted in Figure 2c.<sup>33,34</sup> The ZnO microstructure usually has a growth preferential in the  $\langle 0001 \rangle$  direction; i.e., the growth direction along  $\langle 0001 \rangle$  is normal to the dislocation spiral. When  $v_o$  is less than  $v_c$ , the screw dislocation usually induces the growth of a one-dimensional tube structure.<sup>33</sup> If  $v_o$  is equal to  $v_c$ , all the steps propagate at the same velocity; this similarity in step velocity makes the hillock present a nearly uniform step width and height, which will induce the microstructure of our sample in Figure 1. As shown in Figure 2c, the hillock structure has height  $h$  and width  $\lambda$ . The slope of the hillock  $p = h/\lambda$  is determined by the supersaturation in the growth process.<sup>33</sup>

XRD and EDS were measured to characterize the crystal structure of the ZnO:Sn hillock and testify the existence of Sn elements in the hillock structure. The XRD pattern of the sample shown in Figure 3a revealed that the ZnO:Sn hillock microstructure had a wurtzite crystal structure. No obvious diffraction peaks from  $\text{SnO}_2$ ,  $\text{SnO}$ , and  $\text{ZnSnO}_3$  can be found. The crystal constants were calculated as  $a = 0.324$  nm and  $c = 0.520$  nm. The lattice spacing of ZnO:Sn is a little smaller than that of the pure ZnO, because the ionic radius of  $\text{Sn}^{4+}$  is 0.69 Å, which is smaller than that of  $\text{Zn}^{2+}$  (0.74 Å).<sup>19</sup> The EDS spectrum of the sample is shown in Figure 3b. Typical Zn and O signal peaks can be observed, and weak Sn EDS peaks can be distinguished. According to the element analysis, the atomic contents of Zn, O, and Sn are 49%, 40%, and 0.9%, respectively. The EDS result reveals that only a very low content of Sn is doped in the microstructure.

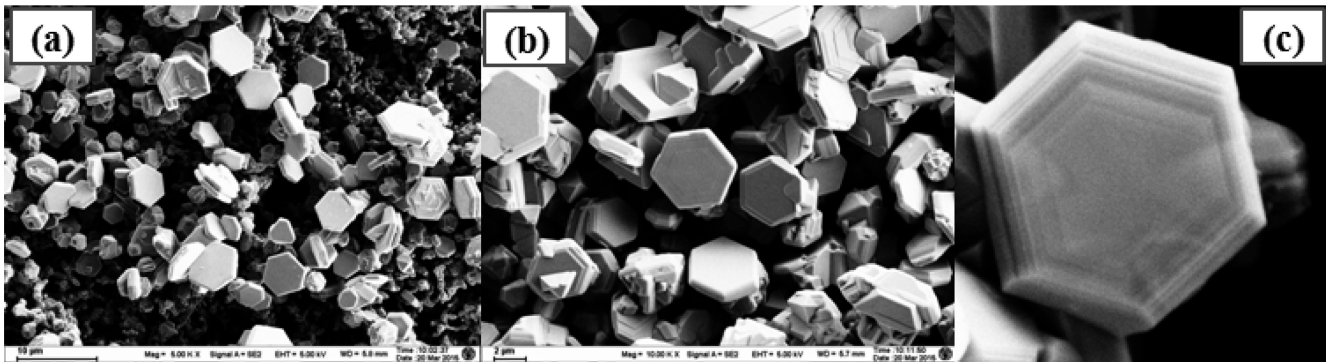
In our experiment, we found that when the Sn content is low, screw dislocation can be found in the ZnO:Sn microstructures, and when the Sn content is more than 10%,  $\text{ZnSnO}_3$  and ZnO/SnO<sub>2</sub> hybrid microstructures will be formed. By increasing the mass of SnO<sub>2</sub> powder in the source materials, ZnO:Sn microstructures with a Sn content of 5.1% are obtained, as shown in Figure 4. Where a lot of ZnO:Sn microdisks were formed, their surfaces also present spiral structures, but the step height is much lower than that shown in Figure 1.

Figure 5a shows the exciton photoluminescence spectrum of the ZnO:Sn hillock microstructure at a temperature of 4 K. The dominant emission peak at 369.5 nm is attributed to the donor-bound exciton (DX) line, and the weak shoulder appearing at 367.08 nm (3.378 eV) originates from free exciton (FX) emission of ZnO:Sn.<sup>35–37</sup> Two other emission bands at 3.307 and 3.236 eV are located at the lower energy side with an



**Figure 3.** XRD (a) and EDS (b) patterns of the ZnO:Sn hillock microstructure.

interval of about 71 meV, and the emission band at 3.307 eV is also lower than that of the free exciton with a 71 meV energy gap, so the peaks at 3.307 and 3.236 eV can be attributed to the longitudinal optical photon replicas of the free excitons, i.e., 1-LO and 2-LO phonon replicas of the free exciton. From the low-temperature PL spectra, we can find that the band gap of the ZnO:Sn microstructure has a value similar to that of the undoped ZnO micro/nanostructures. This indicates that a very low content of Sn doping does not change its band gap. Furthermore, the PL spectra were studied within a temperature range of 4–260 K. With the temperature increasing, the free exciton emission intensity increases and shifts to the lower energy side; meanwhile, the DX, 1-LO, and 2-LO photon replica emission intensities decrease, and their emission bands are broadened due to the exciton thermal delocalization effect. Eventually the FX and DX emission bands are broadened and mixed together to form a single UV emission band when the temperature is increased to room temperature. The inset of Figure 5a shows the whole PL spectrum of the sample at room temperature. Except for the exciton emission band, the PL spectrum also shows a visible band at 530 nm which is generally



**Figure 4.** SEM images of ZnO:Sn with Sn doping of about 5.1%.

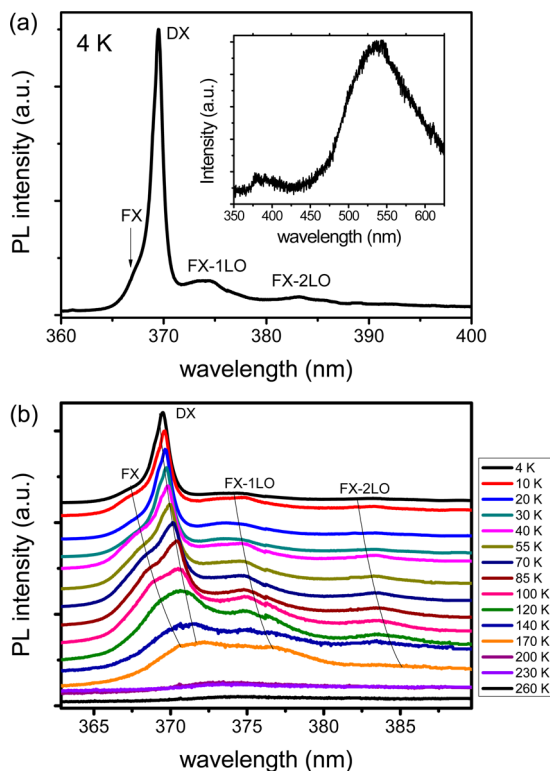


**Figure 5.** (a) Exciton-related recombination emission band at 4 K. The inset is the full emission band of the sample at room temperature. (b) Temperature-dependent PL spectra.

regarded to originate from the oxygen vacancy defect level.<sup>1,38</sup> The defect emission intensity increases with the temperature, but its center wavelength at 530 nm remains unchanged. From the PL result, we can find that the screw-dislocation-induced ZnO:Sn hillock microstructure also contains rich oxygen vacancy defects.

In the following, we mainly discuss the carrier dynamics process in the ZnO:Sn hillock structure. It is well-known that the carrier dynamics process is strongly dependent on the crystal quality. Each kind crystal structure defect, including screw dislocation, point defect and thread defect, can affect the carrier dynamics process. The TRPL of ZnO:Sn hillock structures was measured to characterize the carrier dynamics process.<sup>10,12,35,36</sup> Then TRPL of RS1 and RS2 were measured to compare with that of the ZnO:Sn hillock. The inset of Figure 6 shows the TRPL mapping image of the ZnO:Sn for the exciton emission band. The TRPL mapping image presents a

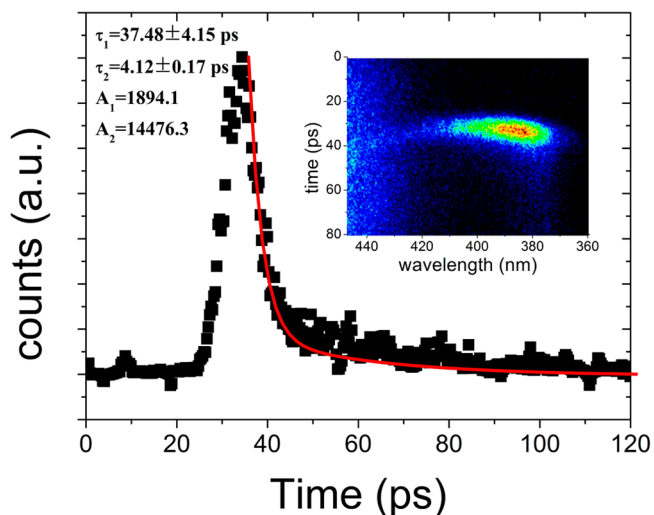


**Figure 6.** Time-resolved PL spectrum of the ZnO:Sn hillock sample. The inset is the corresponding lifetime decay image collected by a streak camera.

very fast decay of the exciton emission. The decay process of the probe wavelength of 383 nm corresponding to the center exciton emission wavelength is plotted in Figure 6. The decay process of ZnO:Sn can be fitted by a biexponential decay function:  $I(t) = A_1 e^{-(t/\tau_1)} + A_2 e^{-(t/\tau_2)}$ , where  $I(t)$  represents the PL intensity as a biexponential function of time,  $A_1$  and  $A_2$  are the relative weights of the two exponential decays with time constants  $\tau_1$  and  $\tau_2$ , respectively. From the fitting curves, the estimated decay time constants  $\tau_1$  and  $\tau_2$  are  $4.12 \pm 0.17$  and  $37.48 \pm 4.15$  ps. In general, the exciton lifetime reflects the decreased rate of population of the excited states.<sup>35,37</sup> Previous reports revealed that the exciton lifetime ranges from tens to hundreds of picoseconds for different ZnO samples. Generally, the longer decay might correspond to the bound exciton recombination, while the shorter decay is attributed to the free exciton recombination. At room temperature the UV emission band is mainly dominated by the free exciton recombination. The exciton decay fitting result shows the weight of the faster lifetime of 4.12 ps is much larger than that of the slow lifetime of 37.48 ps, which indicates that the fast lifetime of 4.12 ps is attributed to free exciton recombination, and the slow lifetime of 37.48 ps originates from bound exciton recombination. Here the lifetime of the free exciton is much faster than the previously reported results. The above SEM and PL results have revealed that the ZnO:Sn microstructure contains both screw dislocation and oxygen vacancy defects. Screw dislocation

and oxygen vacancy defects can quench the exciton emission and provide fast decay channels for exciton recombination. To distinguish the effect of the screw dislocation and oxygen vacancy defects on the carrier dynamics, two reference samples (RS1, RS2) of the ZnO nanorod array without screw dislocation were fabricated. Actually, the ZnO:Sn microstructure without screw dislocation is the best reference sample for discussing the effect of screw dislocation on the carrier dynamics, but we found that the screw dislocation is very easily formed even if an extremely low content of Sn is doped in ZnO. Therefore, the TRPL spectra of the undoped ZnO samples were studied for comparison with that of the screw-dislocation-induced ZnO:Sn hillock microstructure. As shown in Figure 7a, RS1 fabricated at higher oxygen flow shows a strong UV emission peak at 390 nm and a weak broad defect emission at 525 nm, which indicates that RS1 has a lower oxygen vacancy defect density than that in the ZnO:Sn hillock structure. The insets show the cross-section and top-view SEM images of RS1, which present a perfect ZnO nanorod array structure with typically regular hexagonal cross-sections without screw dislocation. Figure 7b shows the PL spectrum of RS2 fabricated at low oxygen flow. The PL spectrum shows a very strong emission band at 530 nm. This indicates that RS2 has a high oxygen vacancy defect density. Figure 7c shows the TRPL spectrum of RS1 at the exciton emission wavelength. The carrier decay process is also fitted by a biexponential function with  $\tau_1 = 13.82 \pm 0.02$  ps and  $\tau_2 = 127.6 \pm 0.35$  ps. Similarly, these two decay processes correspond to free exciton and bound exciton recombination, respectively. Obviously, the exciton decay time of the reference sample is much longer than that of the ZnO:Sn hillock structure. Figure 7d shows the TRPL spectra of RS2 with a high oxygen vacancy defect density. The inset shows the TRPL mapping of RS2. The decay process for the exciton emission wavelength at 390 nm contains two decay time constants,  $\tau_1 = 11.58 \pm 0.01$  ps and  $\tau_2 = 95.52 \pm 0.19$  ps, which are shorter than those of RS1, but a little longer than those of the ZnO:Sn hillock structure. From the TRPL spectra of RS1 and RS2, we can conclude that oxygen vacancy defects can shorten the exciton lifetime. Both oxygen defects and screw dislocation can shorten the lifetime of the carrier,<sup>7</sup> and here, screw dislocation of the ZnO:Sn microstructure further hastens the exciton decay process.

The doping of Sn in ZnO can increase the carrier density and reduce the resistance.<sup>39,40</sup> This can facilitate its application in laser and light-emitting devices. On the basis of the photoluminescence experiment, we further investigate if the lasing emission can be obtained under focused excitation. By focusing the excitation laser spot at the center of the top surface of the selected microhillock, the UV lasing emission from the ZnO:Sn hillock is observed, as shown in Figure 8. When the excitation power density is less than 500 KW/cm<sup>2</sup>, the spectrum shows a broad spontaneous emission band centered at 393 nm. When the excitation power density is increased to 550 KW/cm<sup>2</sup>, three clear sharp emission peaks appear at 392.13, 392.73, and 393.43 nm, respectively, and more peaks emerge as the excitation power is further increased to 750 KW/cm<sup>2</sup>. Such an optical phenomenon is attributed to lasing action in the hillock. In the traditional ZnO microstructure with a perfect hexagonal cross-section, usually whispering gallery mode (WGM) lasing can be formed, where the WGM is formed by the multiple internal reflection induced hexagonal optical loop path.<sup>20,21</sup> However, in the present case, ZnO:Sn shows a deformed hexagonal cross-section for the screw

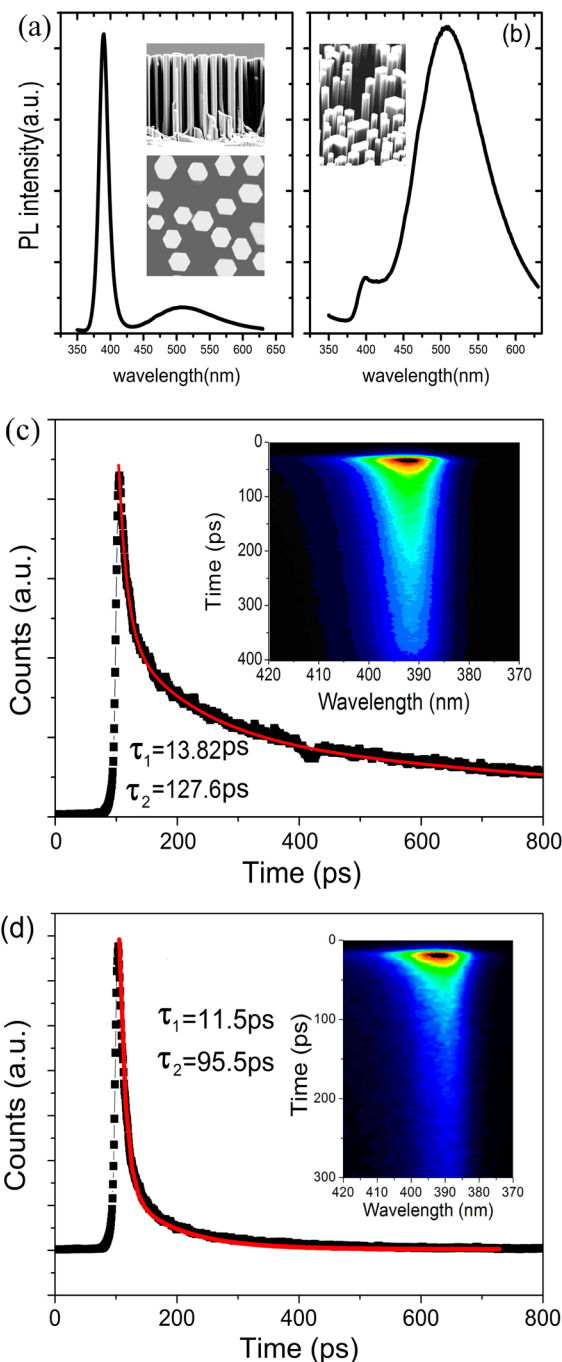


**Figure 7.** (a, b) PL spectrum of the reference samples RS1 and RS2. The insets are the SEM images of the reference samples. (c) Time-resolved PL spectrum of RS1. The inset is the corresponding lifetime decay image collected by a streak camera. (d) Time-resolved PL spectrum of RS2. The inset is the corresponding lifetime decay image collected by a streak camera.

dislocation effect, so the WGM laser optical resonator cavity structure is unachievable. From the SEM result, the height between the top and bottom parallel facets of the microhillock is about 4  $\mu\text{m}$ . It is reasonable to attribute the lasing mode to the vertical Fabry–Perot mode (FPM) generated between the top and bottom surfaces of the ZnO:Sn hillock microstructure.<sup>9</sup> The excited area of the ZnO:Sn hillock is only of about 1  $\mu\text{m}$  radius. Only the FP mode in the excited area can be formed. The schematic optical resonant path in the hillock is shown in

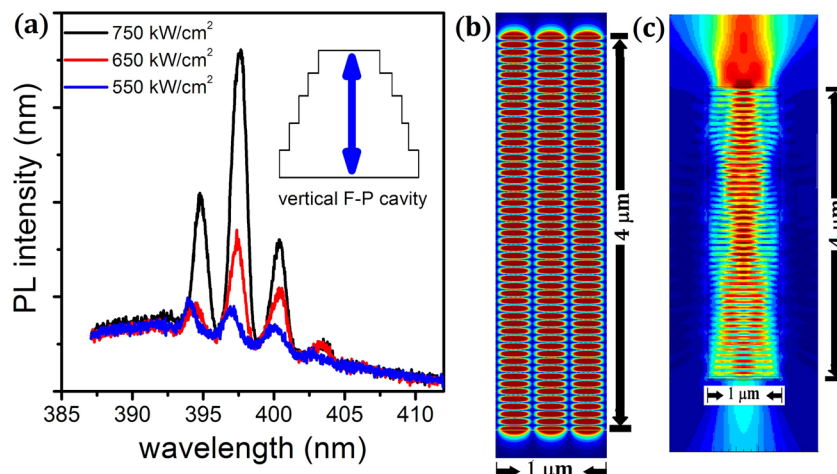


**Figure 8.** (a) Lasing spectra from the ZnO:SnO hillock microstructure. The inset is the schematic graph of the vertical FP lasing cavity. (b) Standing optical wave intensity distribution for the lasing wavelength of 395 nm in a cavity of 4  $\mu\text{m}$  length and 1  $\mu\text{m}$  diameter. (c) Light distribution and transport pattern in the FP cavity.

the inset of Figure 8. The Fabry–Perot mode spacing is given by  $\Delta\lambda = \lambda^2/(2L(n - \lambda(dn/d\lambda)))$ , where  $L$  is the cavity length,  $n$  is the refractive index of the ZnO medium, and  $dn/d\lambda$  is the dispersion relation. The mode spacing between two adjacent cavity modes is 2.7 nm according to the measured lasing spectrum. Using the dispersion of ZnO, the corresponding refractive index is  $n = 2.4$ , and  $\lambda(dn/d\lambda) = -0.012$  at the wavelength of 397.59 nm. The cavity length  $L$  is calculated to be 4.1  $\mu\text{m}$ , which agrees with the height of the hillock structure. By using the finite-difference time-domain (FDTD) method,<sup>37</sup> the optical field distribution in the vertical FP microcavity was simulated. For simplicity, a rectangular region of  $4 \times 1 \mu\text{m}^2$  was constructed as the FP cavity. The length of 4  $\mu\text{m}$  corresponds to the height of the ZnO:Sn hillock, and the width of 1  $\mu\text{m}$  corresponds to the diameter of the excited region. Figure 8b shows the electrical field distribution of the optical resonance mode in the ZnO FP microcavity. The wavelength is 390.5 nm, which is one of the resonance wavelengths of this FP microcavity. It can be seen that a clear standing-wave pattern of the photon oscillation was formed in the cavity. Figure 8c shows the simulated optical intensity distribution of light at a wavelength of 390.5 nm. In the simulation, a linearly polarized plane Gaussian light beam with a width of 5 nm was projected on the top of the vertical FP cavity. We can clearly see that the light intensity in the cavity presents a periodic pattern distribution inside the cavity, which is due to the optical resonance effect. In addition, most of the light emits from the top surface; this is because the FP cavity has a high optical transmittance, so most of the light emits from the top air/ZnO interface. In addition, the lifetimes and the lasing action were also measured (see Figure 9) in the ZnO:Sn sample shown in Figure 4. The lifetimes of free and bound excitons are 2.86 and 18.47 ps, respectively, which also present a very fast photon decay process. The above experimental and numerical results prove that the ZnO:Sn microstructure can still have a perfect UV lasing gain medium, so ZnO:Sn can be used as the candidate material for UV lasers.

#### 4. CONCLUSIONS

In summary, we reported a vapor-phase transport method to realize the screw-dislocation-driven growth of the ZnO:Sn hillock microstructures. The detailed morphology and structure

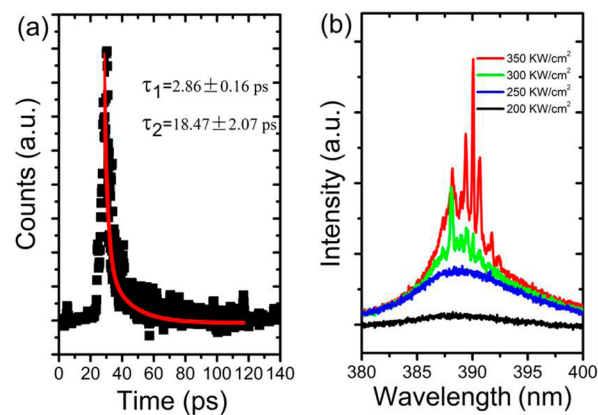


**Figure 9.** TRPL spectrum (a) and lasing spectra (b) from the sample shown in Figure 4.

of ZnO:Sn were characterized, and a screw dislocation growth mechanism was proposed to explain the growth process of the ZnO:Sn hillock structure. The exciton photoluminescence property was discussed using the temperature-dependent photoluminescence spectral technique, and the free and bound exciton lifetimes (4.12 and 37.48 ps) were measured by the time-resolved photoluminescence technique. To demonstrate the effect of oxygen vacancies and screw dislocation on the carrier dynamics, a reference sample of the ZnO nanorod array was investigated. The comparison result reveals that the oxygen vacancies and screw dislocation in the ZnO:Sn hillock play critical roles in shortening the lifetime of the exciton. In addition, the UV lasing action in the ZnO:Sn microstructure and the numerical simulation of the Fabry–Perot lasing mechanism were demonstrated. There, the result is significant for further investigating the optical property and its application to ZnO-based material.

#### AUTHOR INFORMATION

##### Corresponding Authors

\*E-mail: daijun@just.edu.cn.

\*E-mail: guning@seu.edu.cn.

\*E-mail: xcxeu@seu.edu.cn.

**Notes**

The authors declare no competing financial interest.

**ACKNOWLEDGMENTS**

We gratefully appreciate Prof. Shufeng Wang from the Ultrafast Optics Lab of Peking University for helping us to measure the time-resolved photoluminescence spectra. This work was supported by the National Natural Science Foundation of China (NSFC) (Grants 11104119, 11304128, and 61275054), “973” Program (Grants 2013CB932903 and 2011CB302004), and Qinglan Project of Jiangsu Province, Open Funding of State Key Laboratory of Bioelectronics, China Postdoctoral Science Foundation (Grant 2014M551485).

**REFERENCES**

- (1) Burton, W. K.; Cabrera, N.; Frank, F. C. The Growth of Crystals and the Equilibrium Structure of the Surfaces. *Philos. Trans. R. Soc. London, A* **1951**, *243*, 299–358.
- (2) Qian, W.; Rohrer, G. S.; Skowronski, M.; Doverspike, K.; Rowland, L. B.; Gaskill, D. K. Open-Core Screw Dislocation in GaN Epilayers Observed by Scanning Force Microscopy and High-Resolution Transmission Electron-Microscopy. *Appl. Phys. Lett.* **1995**, *67*, 2284–2286.
- (3) Cherns, D.; Henley, S. J.; Ponce, F. A. Edge and Screw Dislocations as Nonradiative Centers in InGaN/GaN Quantum Well Luminescence. *Appl. Phys. Lett.* **2001**, *78*, 2691–2693.
- (4) Hsu, J. W. P.; Manfra, M. J.; Molnar, R. J.; Heying, B.; Speck, J. S. Direct Imaging of Reverse-Bias Leakage through Pure Screw Dislocations in GaN Films Grown by Molecular Beam Epitaxy on GaN Templates. *Appl. Phys. Lett.* **2002**, *81*, 79–81.
- (5) Lei, H. P.; Chen, J.; Ruterana, P. Role of c-Screw Dislocations on Indium Segregation in InGaN and InAlN Alloys. *Appl. Phys. Lett.* **2010**, *96*, 161901.
- (6) Song, J.; Xu, F. J.; Yan, X. D.; Lin, F.; Huang, C. C.; You, L. P.; Yu, T. J.; Wang, X. Q.; Shen, B.; Wei, K.; Liu, X. Y. High Conductive Gate Leakage Current Channels Induced by Segregation around Screw- and Mixed-Type Threading Dislocations in Lattice-Matched  $\text{In}_x\text{Al}_{1-x}\text{N}/\text{GaN}$  Heterostructures. *Appl. Phys. Lett.* **2010**, *97*, 232106.
- (7) Xie, J.; Ozgur, U.; Fu, Y.; Ni, X.; Morkoc, H.; Inoki, C. K.; Kuan, T. S.; Foreman, J. V.; Everitt, H. O. Low Dislocation Densities and Long Carrier Lifetimes in GaN Thin Films Grown on a  $\text{SiNi}_x$  Nanonetwok. *Appl. Phys. Lett.* **2007**, *90*, 041107.
- (8) Bagnall, D. M.; Chen, Y. F.; Zhu, Z.; Yao, T.; Koyama, S.; Shen, M. Y.; Goto, T. Optically Pumped Lasing of ZnO at Room Temperature. *Appl. Phys. Lett.* **1997**, *70*, 2230–2232.
- (9) Huang, M. H.; Mao, S.; Feick, H.; Yan, H. Q.; Wu, Y. Y.; Kind, H.; Weber, E.; Russo, R.; Yang, P. D. Room-Temperature Ultraviolet Nanowire Nanolasers. *Science* **2001**, *292*, 1897–1899.
- (10) Theuring, M.; Vehse, M.; von Maydell, K.; Agert, C. AZO-Ag-AZO Transparent Electrode for Amorphous Silicon Solar Cells. *Thin Solid Films* **2014**, *558*, 294–297.
- (11) Shei, S. C. Multiple Nanostructures on Full Surface of GZO/GaN-Based LED To Enhance Light-Extraction Efficiency Using a Solution-Based Method. *IEEE J. Quantum Electron.* **2014**, *50*, 629–632.
- (12) Chen, H. T.; Cao, Y.; Zhang, J. L.; Zhou, C. W. Large-Scale Complementary Macroelectronics Using Hybrid Integration of Carbon Nanotubes and IGZO Thin-Film Transistors. *Nat. Commun.* **2014**, *5*, 4097.
- (13) Li, X.; Geng, D.; Mativenga, M.; Jang, J. High-Speed Dual-Gate a-IGZO TFT-Based Circuits with Top-Gate Offset Structure. *IEEE Electron Device Lett.* **2014**, *35*, 461–463.
- (14) Ortega, Y.; Fernandez, P.; Piqueras, J. Growth and Luminescence of Oriented Nanoplate Arrays in Tin Doped ZnO. *Nanotechnology* **2007**, *18*, 115606.
- (15) Ortega, Y.; Fernandez, P.; Piqueras, J. Self-Assembled Tin-Doped ZnO Nanowire and Nanoplate Structures Grown by Thermal Treatment of ZnS Powder. *J. Cryst. Growth* **2009**, *311*, 3231–3234.
- (16) Shelke, V.; Sonawane, B. K.; Bhole, M. P.; Patil, D. S. Electrical and Optical Properties of Transparent Conducting Tin Doped ZnO Thin Films. *J. Mater. Sci.* **2012**, *23*, 451–456.
- (17) Shishyanu, S. T.; Shishyanu, T. S.; Lupan, O. I. Sensing Characteristics of Tin-Doped ZnO Thin Films as  $\text{NO}_2$  Gas Sensor. *Sens. Actuators, B* **2005**, *107*, 379–386.
- (18) Deng, R.; Zhang, X. T. Effect of Sn Concentration on Structural and Optical Properties of Zinc Oxide Nanobelts. *J. Lumin.* **2008**, *128*, 1442–1446.
- (19) Jung, M.; Kim, S.; Ju, S. Enhancement of Green Emission from Sn-Doped ZnO Nanowires. *Opt. Mater.* **2011**, *33*, 280–283.
- (20) Czekalla, C.; Sturm, C.; Schmidt-Grund, R.; Cao, B.; Lorenz, M.; Grundmann, M. Whispering Gallery Mode Lasing in Zinc Oxide Microwires. *Appl. Phys. Lett.* **2008**, *92*, 241102.
- (21) Dai, J.; Xu, C. X.; Zheng, K.; Lv, C. G.; Cui, Y. P. Whispering Gallery-Mode Lasing in ZnO Microrods at Room Temperature. *Appl. Phys. Lett.* **2009**, *95*, 241110.
- (22) Dai, J.; Xu, C. X.; Sun, X. W. ZnO-Microrod/p-GaN Heterostructured Whispering-Gallery-Mode Microlaser Diodes. *Adv. Mater.* **2011**, *23*, 4115–4119.
- (23) Goldberger, J.; Sirbuly, D. J.; Law, M.; Yang, P. ZnO Nanowire Transistors. *J. Phys. Chem. B* **2005**, *109*, 9–14.
- (24) Hoffman, R. L.; Norris, B. J.; Wager, J. F. ZnO-Based Transparent Thin-Film Transistors. *Appl. Phys. Lett.* **2003**, *82*, 733–735.
- (25) Wang, X.; Zhou, J.; Song, J.; Liu, J.; Xu, N.; Wang, Z. L. Piezoelectric Field Effect Transistor and Nanoforce Sensor Based on a Single ZnO Nanowire. *Nano Lett.* **2006**, *6*, 2768–2772.
- (26) Hu, L.; Yan, J.; Liao, M.; Xiang, H.; Gong, X.; Zhang, L.; Fang, X. S. An Optimized Ultraviolet-A Light Photodetector with Wide-Range Photoresponse Based on ZnS/ZnO Biaxial Nanobelt. *Adv. Mater.* **2012**, *24*, 2305–2309.
- (27) Law, J. B. K.; Thong, J. T. L. Simple Fabrication of a ZnO Nanowire Photodetector with a Fast Photoresponse Time. *Appl. Phys. Lett.* **2006**, *88*, 133114.
- (28) Soci, C.; Zhang, A.; Xiang, B.; Dayeh, S. A.; Aplin, D. P. R.; Park, J.; Bao, X. Y.; Lo, Y. H.; Wang, D. ZnO Nanowire UV Photodetectors with High Internal Gain. *Nano Lett.* **2007**, *7*, 1003–1009.
- (29) Xu, C. X.; Sun, X. W.; Dong, Z. L.; Yu, M. B. Zinc Oxide Nanodisk. *Appl. Phys. Lett.* **2004**, *85*, 3878–3880.
- (30) Morin, S. A.; Bierman, M. J.; Tong, J.; Jin, S. Mechanism and Kinetics of Spontaneous Nanotube Growth Driven by Screw Dislocations. *Science* **2010**, *328*, 476–480.
- (31) Northrup, J. E. Screw Dislocations in GaN: The Ga-Filled Core Model. *Appl. Phys. Lett.* **2001**, *78*, 2288–2290.
- (32) Kioseoglou, J.; Kalesaki, E.; Belabbas, I.; Chen, J.; Nouet, G.; Komninou, P.; Karakostas, T. Effect of Doping on Screw Threading Dislocations in AlN and Their Role as Conductive Nanowires. *Phys. Status Solidi C* **2012**, *9*, 484–487.
- (33) Meng, F.; Morin, S. A.; Forticaux, A.; Jin, S. Screw Dislocation-Driven Growth of Nanomaterials. *Acc. Chem. Res.* **2013**, *46*, 1616–1626.
- (34) Morin, S. A.; Forticaux, A.; Bierman, M. J.; Jin, S. Screw Dislocation-Driven Growth of Two-Dimensional Nanoplates. *Nano Lett.* **2011**, *11*, 4449–4455.
- (35) Xing, G. Z.; Wang, D. D.; Yao, B.; Nien, A. Q. L. F.; Yan, Y. S. Structural Characteristics, Low Threshold Ultraviolet Lasing and Ultrafast Carrier Dynamics in High Crystalline ZnO Nanowire Arrays. *Chem. Phys. Lett.* **2011**, *515*, 132–136.
- (36) Johnson, J. C.; Knutson, K. P.; Yan, H. Q.; Law, M.; Zhang, Y. F.; Yang, P. D.; Saykally, R. J. Ultrafast Carrier Dynamics in Single ZnO Nanowire and Nanoribbon Lasers. *Nano Lett.* **2004**, *4*, 197–204.
- (37) Zhang, X. H.; Chua, S. J.; Yong, A. M.; Yang, H. Y.; Lau, S. P.; Yu, S. F.; Sun, X. W.; Miao, L.; Tanemura, M.; Tanemura, S. Exciton

Radiative Lifetime in ZnO Nanorods Fabricated by Vapor Phase Transport Method. *Appl. Phys. Lett.* **2007**, *90*, 013107.

(38) Dong, H. X.; Liu, Y.; Lu, J.; Chen, Z. H.; Wang, J.; Zhang, L. Single-Crystalline Tower-like ZnO Microrod UV Lasers. *J. Mater. Chem. C* **2013**, *1*, 202–206.

(39) Ajili, M.; Castagne, M.; Turki, N. K. Study on the Doping Effect of Sn-Doped ZnO Thin Films. *Superlattices Microstruct.* **2013**, *53*, 213–222.

(40) Ilıcan, S.; Caglar, M.; Caglar, Y. Sn Doping Effects on the Electro-Optical Properties of Sol Gel Derived Transparent ZnO Films. *Appl. Surf. Sci.* **2010**, *256*, 7204–7210.